Bull. Mater. Sci. (2021)44:154
https://doi.org/10.1007/s12034-021-02453-y

Synthesis, physicochemical and photocatalytic activities of nano $ZnCo_2O_4$ catalyst for photodegradation of various dyes under sunlight irradiation

S HEMAMALINI and R MANIMEKALAI*
Department of Chemistry, Kongunadu Arts and Science College, Coimbatore 641 029, India
*Author for correspondence (rmanimekalai04@gmail.com)

MS received 2 October 2020; accepted 26 January 2021

Abstract. The transition metal (Zn^{2+})-doped Co_3O_4 nanoparticle was tailored through thermal decomposition of precursor synthesized by simple co-precipitation which is an experimentally and economically comfortable method. The precursor was characterized using EDS, FTIR and thermogravimetric analysis. Also, the nano-sized metal oxide synthesized from its precursor was investigated by powder X-ray diffraction, X-ray photoelectron spectroscopy, high-resolution transmission electron microscopy, scanning electron microscopy. The specific surface area was scrutinized through Bruner–Emmet–Teller (BET) adsorption. The ferromagnetic property of the nanoparticle was detected using vibrating sample magnetometer. The photocatalytic degradation performance of nano $ZnCo_2O_4$ was evaluated using methyl orange (MO), rhodamine B (RhB) and Congo red (CR) dyes under sunlight. The nanoparticle demonstrated good photocatalytic activity towards azo dyes (MO and CR) rather than rhodamine (RhB)-based dye. The degradation of organic dyes was found to follow first-order kinetics.

Keywords. Transition metal; co-precipitation; ferromagnetic; photocatalytic activity.

1. Introduction

Today, environmental pollution and water scarcity have become a major threat to social and economic growth in developing countries. Modernization and industrialization have also led to the discharge of different types of toxic dye wastes, which cannot be removed by traditional sewage treatment [1–5]. Methyl orange (MO), Congo red (CR) and rhodamine B (RhB) dyes are commonly used in textile, food, paint, leather and cosmetic industries. These hazardous dye wastes from the industries can produce toxic by-products which cause severe health risks for humankind, animals and aquatic life [6,7].

There are numerous types of physical and chemical methods available for treating coloured wastewater. However, it is difficult to degrade toxic dyes by choosing feasible techniques [8,9]. Currently, the role of semiconductor photocatalysts in the degradation of organic dyes has attracted more attention due to their simple preparation, non-toxicity and photostability [10–12]. The heterogeneous transition metal oxides with general spinel structure AB_2O_4 (where A and B can be bivalent and trivalent, respectively) were reported that they were able to manage the effluent waste effectively due to their unique physical, chemical and optical properties. The transition metal dopants can create oxygen vacancies which are also delaying the e^-/h^+ pair recombination process [13–15]. Different transition metals, such as Co, Zn, Fe, Cu, Ni and Ag-doped semiconductor photocatalysts were reported for their enhanced photocatalytic efficiencies for the degradation of organic and inorganic pollutants [16–21]. However, the comparative analysis on the degradation of different dyes in the presence of $ZnCo_2O_4$ catalyst synthesized by simple co-precipitation has not been reported.

We report the structural, textural, magnetic, optical properties and photocatalytic efficiency of the nano $ZnCo_2O_4$ catalyst. In the present study, nano $ZnCo_2O_4$ was synthesized by a simple coprecipitation–calcination route by employing $[Zn_{0.75}Co_{2.25}(PhOAc)_2(N_2H_4)_2]$ as a cobalt precursor. The decomposition of hydrazine content present in the precursor liberates energy in the form of heat which produces voluminous ultrafine metal oxides at relatively lower temperatures [22–25]. We observed the simple formation of nano $ZnCo_2O_4$ from the cobaltous phenoxyacetate hydrazinate precursor, but the formation of oxides synthesized from unhydrazinated precursor, needs rigorous temperature [26,27]. It has been reported that the hydrazinated metal carboxylates and mixed metal carboxylates yield spinels with a high surface area which must be attributed to the smaller size effect of the

Published online: 24 May 2021

nanoparticles. Hence, these precursors are important in the preparation of nanosized materials which can have remarkable magnetic, biological and catalytic applications [28–31].

2. Experimental

2.1 *Materials and reagents*

The reagents used in this study have been purchased from a local vendor and used without further purification. Phenoxyacetic acid (PhOAc), cobalt nitrate hexahydrate, zinc nitrate hexahydrate, hydrazine hydrate (99%), ethanol, diethyl ether, carbon tetrachloride concentrated hydrochloric acid, CR, RhB and MO dyes were purchased from Sigma Aldrich and Himedia.

2.2 *Preparation of precursor $[Zn_{0.75}Co_{2.25}(PhOAc)_2(N_2H_4)_2]$*

The precursor $[Zn_{0.75}Co_{2.25}(PhOAc)_2(N_2H_4)_2]$ was synthesized by a simple co-precipitation method. In a typical synthesis route, the precursor solution was prepared by dissolving cobalt nitrate hexahydrate (2.25 g, 0.0077 mol) in 50 ml of distilled water. To accomplish transition metal doping, an appropriate amount of zinc nitrate hexahydrate (0.75 g, 0.0025 mol), was added to the precursor solution with constant stirring. The aqueous solution (50 ml) of hydrazine hydrate (2.0 ml, 0.0399 mol) and phenoxyacetic acid (2 g, 0.0131 mol) was added to the aqueous mixture with constant stirring. The obtained mixture was kept aside for 3 h to achieve complete precipitation. The pink precipitate is filtered and washed many times with water, alcohol followed by diethyl ether to remove adsorbed impurities and then, the pink cake is dried at room temperature. The precursor was analysed by EDS, FTIR and TG/DTA analysis.

$$0.75Zn(NO_3)_2{\cdot}6H_2O + 2.25Co(NO_3)_2{\cdot}6H_2O + 2N_2H_4 \cdot H_2O + 2C_6H_5OCH_2COOH \downarrow \left[Zn_{0.75}Co_{2.25}(C_6H_5OCH_2COO)_2(N_2H_4)_2\right] + 2HNO_3.$$

2.3 *Preparation of nano $ZnCo_2O_4$*

Nano $ZnCo_2O_4$, obtained from thermal decomposition of its precursor $[ZnCo(PhOAc)_2(N_2H_4)_2]$ was done by transferring the desiccated precursor to the silica crucible and calcined in a muffle furnace at 400°C for 3 h. The fine black cobaltite crystals were allowed to cool to room temperature and stored in airtight containers.

$$Zn_{0.75}Co_{2.25}(C_6H_5OCH_2COO)_2(N_2H_4)_2 + 41O_2 \xrightarrow{400^\circ C} ZnCo_2O_4 + 16CO_2 + 2N_2 + 11H_2O.$$

This final product was characterized by EDS, FTIR, XRD, SEM, UV-DRS, XPS, PL, BET, TEM and VSM techniques. Synthesis of nano $ZnCo_2O_4$ is illustrated in figure 1.

2.4 *Characterization*

Elemental analysis was done on the Bruker nano GmbH EDS analyzer. The FTIR spectrum of the powdered sample has been recorded from 4000 to 400 cm^{-1} by Shimadzu with pressed KBR pellets.TG/DTA trace was performed on Perkin Elmer STA 6000 thermal analyzer with a heat rating of 20°C min^{-1} at temperature range of room temperature (RT)–700°C. Bruker AXS D8 advance analyzer has been utilized to derive a powder XRD (PXRD) pattern with an angle range of 10–90°. UV–VIS–NIR (Varion Cary 5000) has been carried out to record absorption data. PL spectrum in the range of 200–800 nm at an excitation wavelength of 380 nm was done by Floromax-4 spectrometer. The surface chemical state of the sample was studied by the PHI VersaProbe II XPS analyzer. TEM micrograph and SAED pattern were found by JEOL/JEM 2100 HRTEM analyzer. The morphological and compositional observations were recorded by JOEL JSM-6390LV and OXFORD XMX N. Quantachrome gas sorption system was exploited to find BET surface area. The magnetic measurements of metal oxide were performed by a vibrating sample magnetometer (Lakeshore VSM 7410) at RT. The photodegradation study was carried out using Shimadzu UV-2550 UV–Vis spectrophotometer.

2.5 *Dye degradation study*

The catalytic performance of the sample was detected by catalytic degradation of MO, CR and RhB dyes. Stock solution (500 mg l^{-1}) was prepared by dissolving 0.5 g dye in 1000 ml deionized water. Before the irradiation process, the dye solutions were constantly stirred for about 30 min to

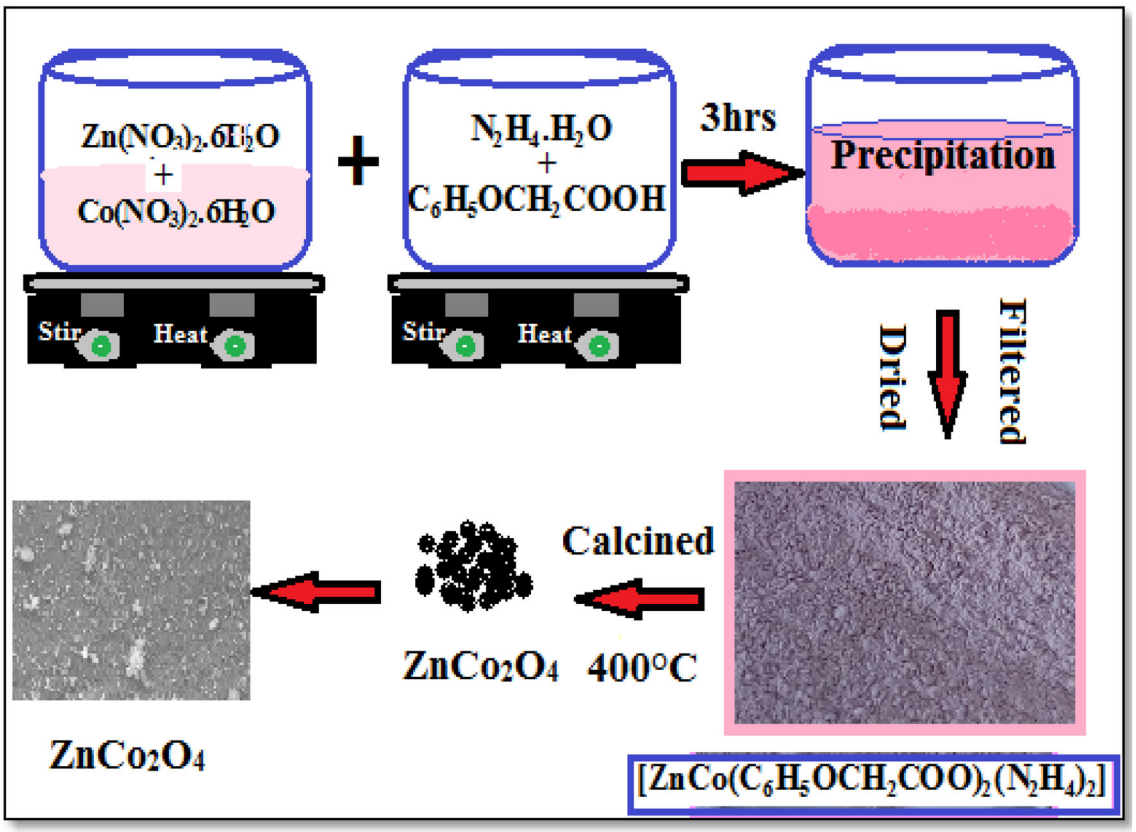

Figure 1. Synthesis of nano $ZnCo_2O_4$ by co-precipitation method.

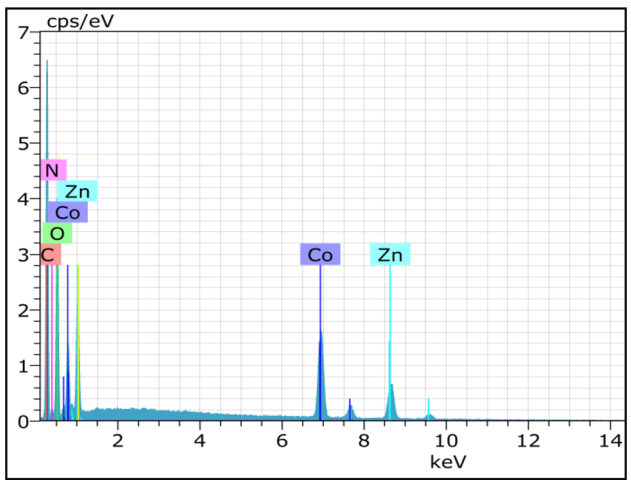

Figure 2. EDS spectrum of the precursor.

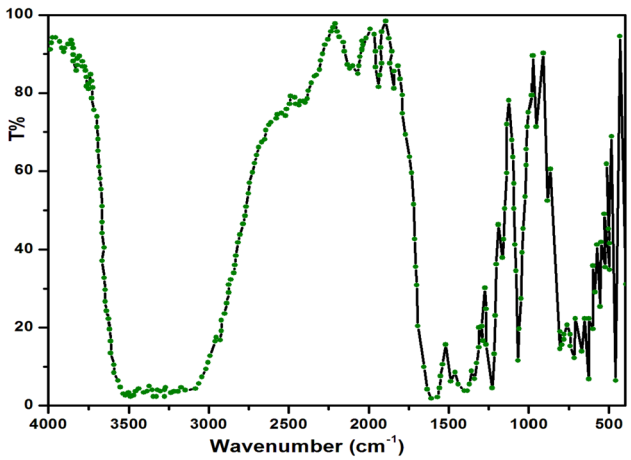

Figure 3. FTIR spectrum of the precursor.

attain adsorption equilibrium between the dye molecules and catalyst surface. Then, the suspension is irradiated in the presence of sunlight at regular time intervals and the degradation process was recorded by UV–Vis spectrophotometer at 464, 497 and 550 nm for MO, CR and RhB, respectively.

3. Results and discussion

3.1 *Characterization of precursor*

The hydrazine content in the precursor was determined by using standard 0.025 M KIO_3 as titrant under Andrew's conditions [32]. Molar ratio of 2:2 was maintained for the aqueous mixture of phenoxy acetate and hydrazine hydrate

in the preparation of the precursor. The analytical data of the precursor was found to be in good agreement with the composition of $[Zn_{0.75}Co_{2.25}(PhOAc)_2(N_2H_4)_2]$. The presence of elements was identified from EDS analysis as shown in figure 2.

Figure 3 shows the FTIR spectrum of the precursor $[Zn_{0.75}Co_{2.25}(PhOAc)_2(N_2H_4)_2]$. The bands in the region of 3204–3328 cm^{-1}, are due to the N–H stretching frequency of hydrazine moiety. The N–N stretching frequency observed at 952 cm^{-1}, proved the bidentate bridging nature of hydrazine. The frequency separation of 262 cm^{-1} shows the difference between asymmetric and symmetric carbonyl stretchings ($\Delta\upsilon = \upsilon_{asym} - \upsilon_{sym}$) which confirms the monodentate coordination of the carboxylate group in the phenoxyacetic acid to the central metal atom [33].

The thermal decomposition of the hydrazine precursor can be determined by TG/DTA trace. As shown in figure 4, four endothermic processes were observed. Weak endothermic peaks observed from 120 to 175°C are attributed to the removal of hydrazine molecules in the precursor [34,35]. The strong endothermic peaks observed at 286.36 and 373.79°C were accompanied by the elimination of two carboxylate groups. No other endothermic peaks were detected, indicating that the organic matter of the precursor has been completely degraded. The thermal analysis result shows the decomposition temperature of $ZnCo_2O_4$ nanoparticles formed at 400°C.

3.2 *Characterization of nano $ZnCo_2O_4$*

3.2a Structural studies: The crystalline nature of the as-prepared sample was precisely resolved by XRD analysis, is shown in figure 5. The diffraction peaks at (220), (311), (222), (400), (331), (422), (511), (440) and (531) are in good agreement with spinel cubic $ZnCo_2O_4$ structure (JCPDS #23-1390) [36], suggesting no secondary phases. The well-ordered peaks of nanoparticles proposed the good crystallinity of the sample [37]. The average particle size was determined by using the Scherrer formula, $d = 0.9\lambda/\beta\cos\theta$, where d, λ, β and θ denote particle size, wavelength of X-ray (1.504 Å), the half-width of highest intensity reflection in radian and angle of reflection. The average crystallite size was found to be 17 nm. The calculated value of the lattice parameter, a = 8.096 Å of nano $ZnCo_2O_4$ is close to the reported value. The FTIR spectra of as-prepared nanoparticle show two absorption bands at 671 and 565 cm^{-1}, indicating stretching vibration of M–O bond in spinel Co_3O_4 metal oxide. The band found at 565 cm^{-1} is ascribed to the vibrations of bond evolved by Co^{3+} ion present in the octahedral holes of the crystal lattice. Another band found at 671 cm^{-1} is attributed to Co^{2+} ion which is present in tetrahedral holes of the lattice [38,39]. Figure 6 shows the FTIR transmission spectrum of nano $ZnCo_2O_4$ nanoparticle and the spectral details are in good agreement

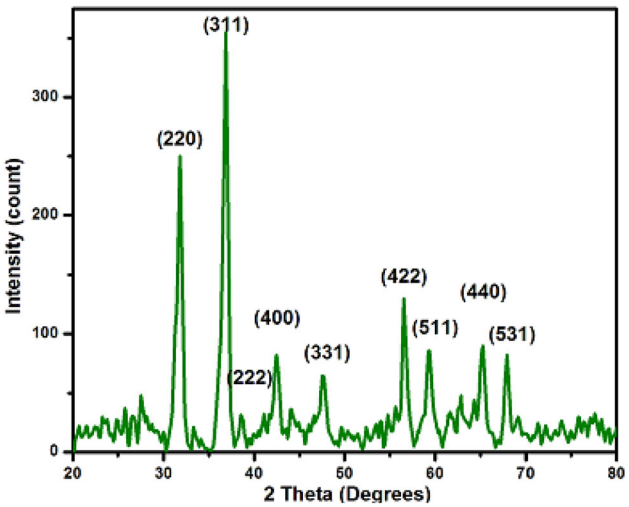

Figure 5. PXRD pattern of nano $ZnCo_2O_4$.

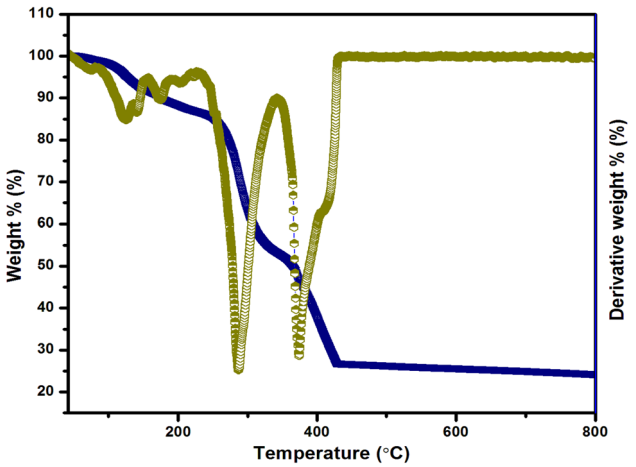

Figure 4. TG/DTG curve of the precursor.

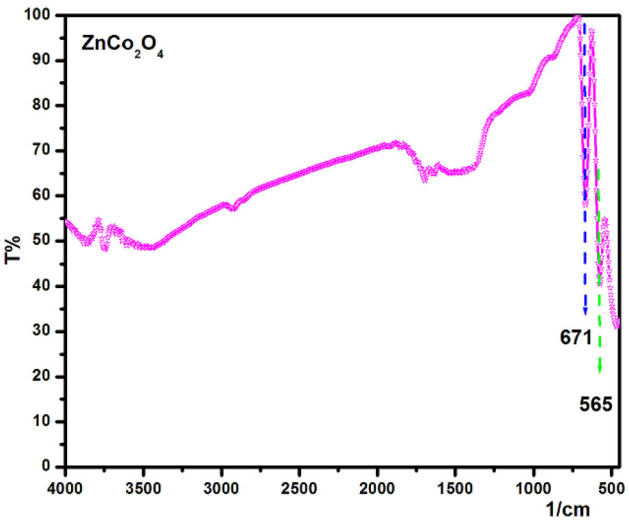

Figure 6. FTIR spectrum of nano $ZnCo_2O_4$.

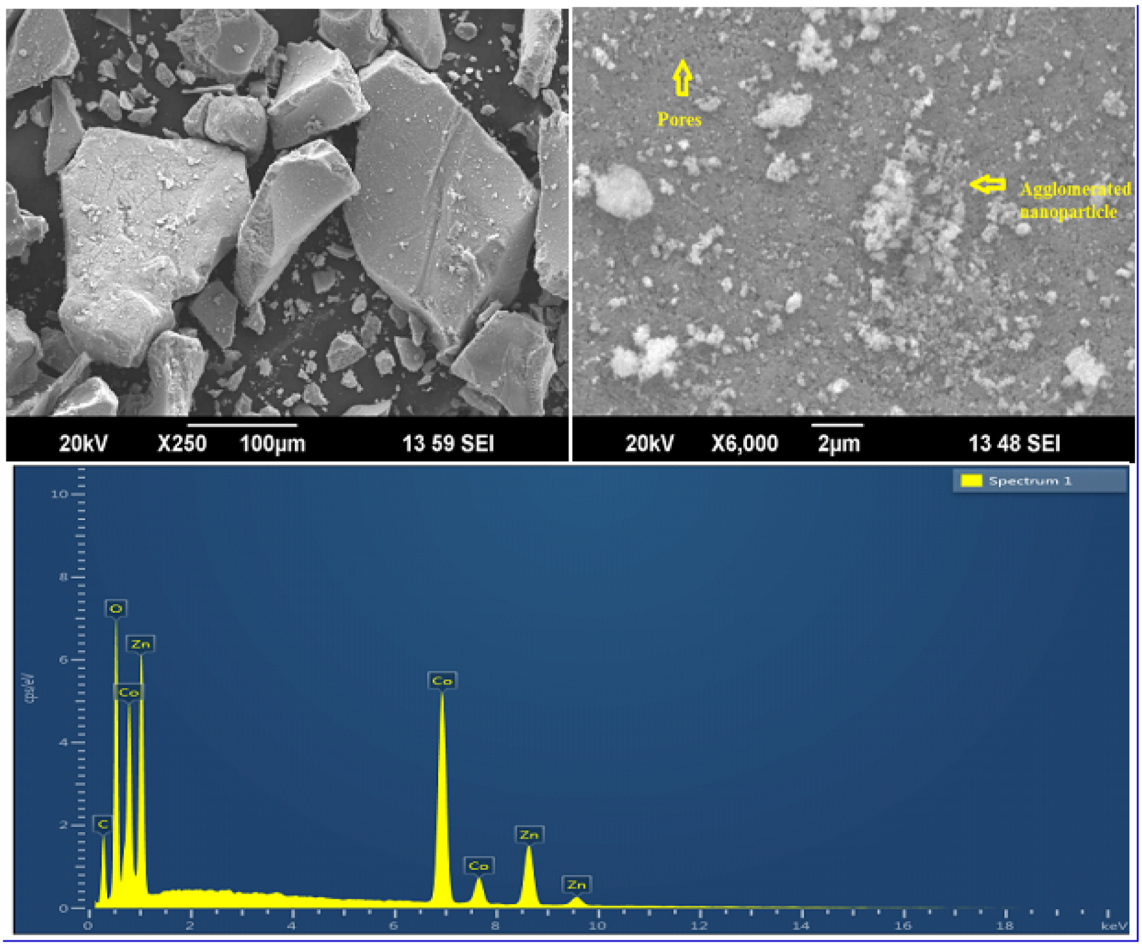

Figure 7. SEM–EDS picture of nano $ZnCo_2O_4$.

with the PXRD results. The SEM micrographs have demonstrated the agglomerated microcrystalline grains with few overgrown particles. To confirm the presence of elements, the EDS analysis was performed and is shown in figure 7.

Figure 8a–d shows the HRTEM images of nano $ZnCo_2O_4$ synthesized by thermal decomposition of $[ZnCo(PhoAc)_2(N_2H_4)_2]$ precursor at 400°C. Corresponding SAED pattern substantiated the polycrystalline nature of the sample. Figure 8b shows SAED rings which are well-matched with spinel $ZnCo_2O_4$ lattice. HRTEM image of nano $ZnCo_2O_4$ shows lattice spacing of 0.4 and 0.24 nm agreed with (111) and (311) planes (figure 8c). The particle size distribution of nanoparticles is shown in figure 8d and it acquires a narrow size distribution of 14–22 nm. The average particle size derived from the TEM image using Image J software is very close to the average particle size determined from the Scherrer formula.

Figure 9 shows N_2 adsorption–desorption isotherm of the prepared sample. According to the IUPAC classification, the shape of nano $ZnCo_2O_4$ isotherm corresponding to type IV and H3 hysteresis loop with specific surface area calculated at about 29 $m^2\ g^{-1}$. The relative pressure ranges from 0.3 to 1, suggesting that the fabricated material is mesoporous [40]. Pore size distribution, demonstrated by the BJH method, is displayed in the inset (figure 9). Fine-sized pores of a radius of about 10.5 nm with a pore volume of 0.078 $cm^3\ g^{-1}$ is observed clearly from figure 9.

The surface chemical state of the as-obtained material was studied by XPS analysis. The survey spectrum of nano $ZnCo_2O_4$ confirms the presence of Zn 2p, Co 2p and O 1s atoms only (figure 10a). Figure 10b shows the XPS spectrum of Zn 2p of $Zn_{3/2}$ and $Zn_{1/2}$ peaks, located at 1021.1 and 1044.4 eV, confirms the presence of Zn (II) oxidation state [41]. The doublet positioned at 779.20 and 780.23 eV are ascribed to Co $2p_{3/2}$, whilst the doublet peaked at 796.03 and 794.75 eV are associated with Co $2p_{1/2}$ (figure 10c). Peaks at 780.23 and 796.03 eV are characteristic of Co^{2+}, while peaks at 779.20 and 794.75 eV are indexed to Co^{3+} ions. Also, the satellite peaks pointed at 803.31 and 786.37 eV, confirms the formation of cobalt (Co^{2+} and Co^{3+}) species [42,43]. Figure 10d shows the O 1s spectrum of $ZnCo_2O_4$ and the contribution at 529.56 eV is related to M–O bonding and the peak at 531.08 eV is attributed to defects in subsurface [44].

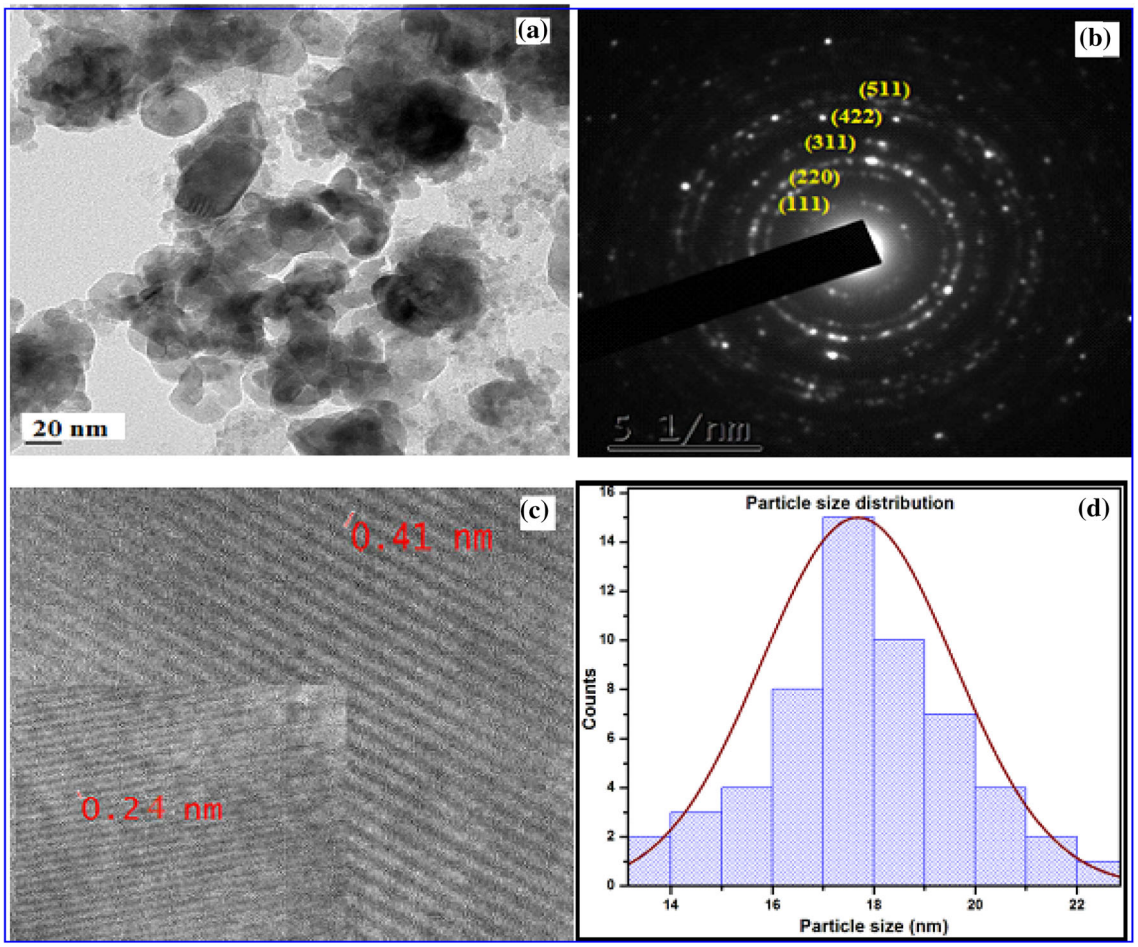

Figure 8. (**a**) HRTEM image, (**b**) SAED pattern, (**c**) image of interplanar spacing and (**d**) particle size distribution of nano $ZnCo_2O_4$.

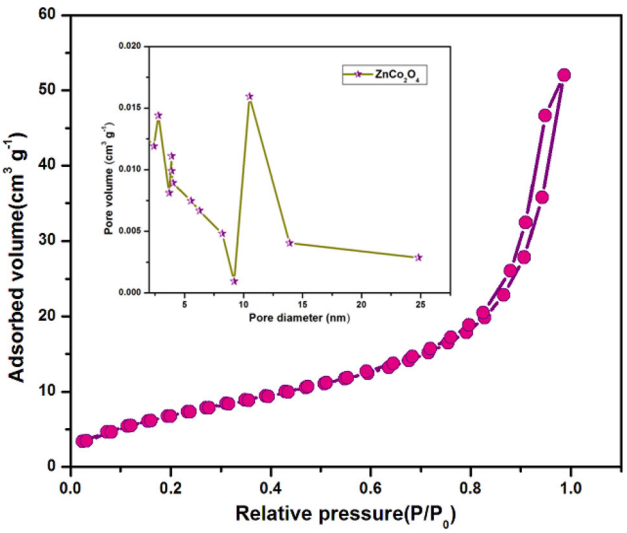

Figure 9. N_2 adsorption–desorption isotherm and BJH pore size distribution curve (inset) of nano $ZnCo_2O_4$.

3.2b Magnetic studies: Figure 11 shows the room-temperature ferromagnetic (RTFM) nature of the prepared material with saturation magnetization (M_s) of 49.928×10^{-3} emu g^{-1}, remanent magnetization (M_r) of 0.0121 emu g^{-1} and coercivity (H_c) of 400 Oe. The magnetic properties of the nanoparticle were supposed to derive from shape, crystallinity, direction of magnetization and so on. The inset (figure 11) shows that the ferromagnetic nano $ZnCo_2O_4$ can be recovered and recycled for application studies.

3.2c Optical studies: The optical absorption spectrum of nano $ZnCo_2O_4$ is shown in figure 12a (inset). The diffuse reflectance UV–visible spectrum of $ZnCo_2O_4$ shows two absorption bands owing to the ligand to metal charge transfer referred as ($O^{-2} \rightarrow Co^{2+}$) and ($O^{-2} \rightarrow Co^{3+}$). The band gap energy of the prepared nanoparticle was determined from the Kubelka–Munk function. According to the transformed Kubelka–Munk relation [45]:

$$F(R) = \frac{K}{S} = \frac{(1-R)^2}{2R}.$$

$F(R)$, Kubelka–Munk function, which is directly proportional to the absorption coefficient K, whereas $K = (1-R)^2$ and inversely proportional to the scattering factor S, $S = 2R$ where R is the diffused reflectance of the material $R = \frac{R\%}{100}$. $(F(R)hv)^2$ *vs.* hv plot gives optical band gap energy

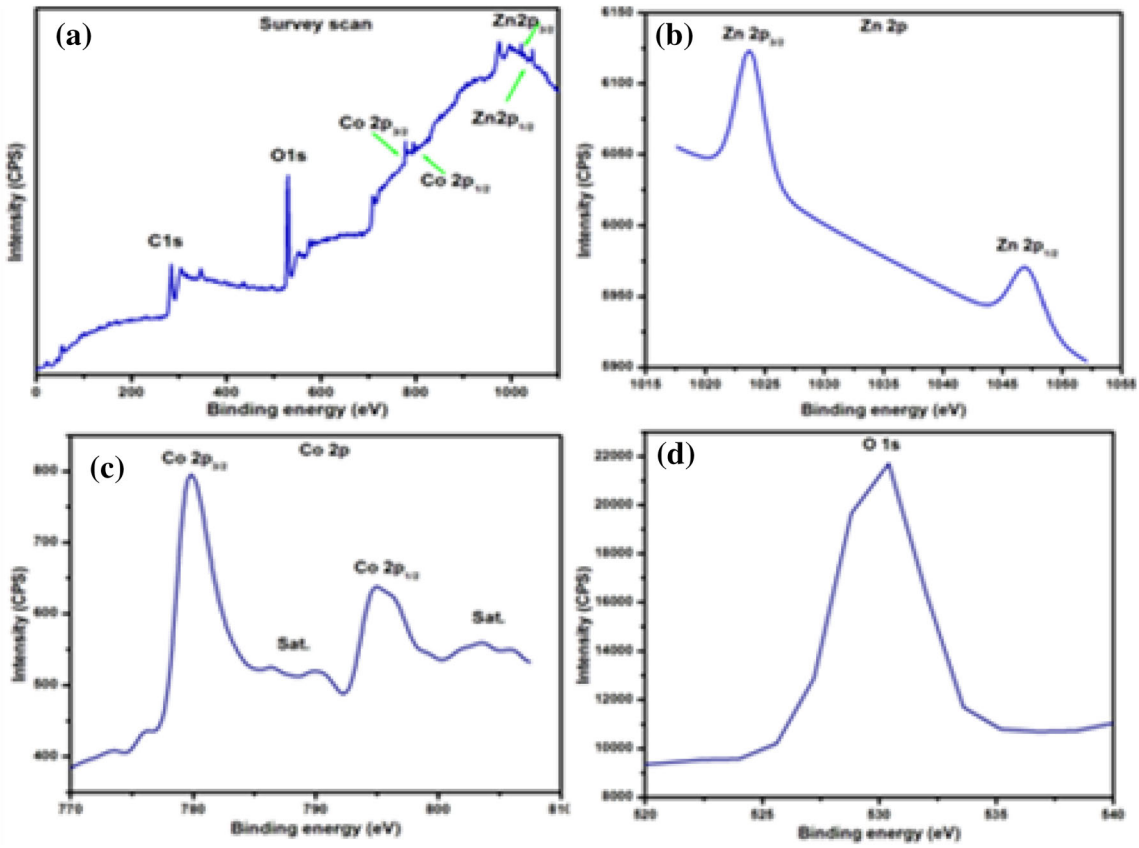

Figure 10. XPS spectra of nano $ZnCo_2O_4$. (**a**) Survey, (**b**) Zn 2p, (**c**) Co 2p and (**d**) O 1s.

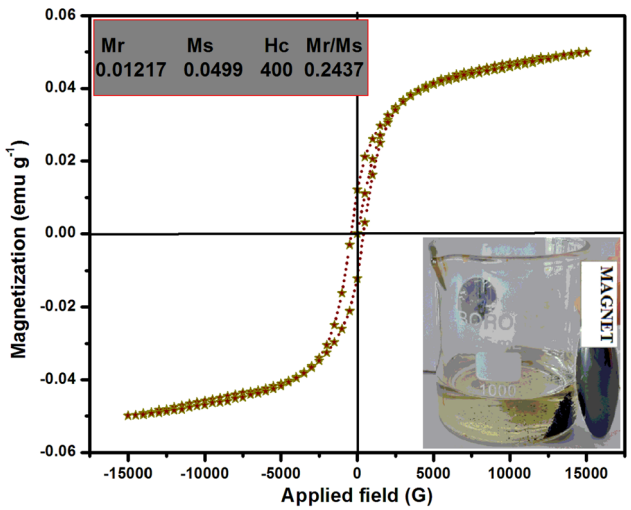

Figure 11. VSM hysteresis loop, magnetic separation (inset) of nano $ZnCo_2O_4$.

of bimetal oxides. The obtained multiple band gaps of nano $ZnCo_2O_4$ are due to the degeneracy of valence band [46] (figure 12a). The photoluminescence spectrum provides information on the band gap and recombination effects. The band observed near 408 nm is due to near band edge emission and the band near blue emission is ascribed to oxygen vacancy (figure 12b).

4. Photocatalytic performance and photodegradation kinetics of nano $ZnCo_2O_4$

4.1 *Catalyst loading*

The as-prepared catalyst is used to degrade MO, CR and RhB dyes under similar experimental conditions in the presence of sunlight. Working solutions of the desired concentration were prepared by successive dilution of the stock solution. To find the optimal catalyst loading, different amounts of the catalyst (20, 40, 60 and 80 mg) were taken for the photocatalytic experiment. The increase in catalyst dosage up to 80 mg, increased the degradation efficiency. Hence, 80 mg of catalyst is found to be optimal for degrading the dye solution.

4.2 *Effect of catalyst*

To explore the catalytic performance, the comparative experiments with different dyes and degradation kinetics were inspected. The degradation efficiency was determined by the following equation:

$$\text{Photodegradation}\,\% = \frac{C_0 - C}{C_0}.$$

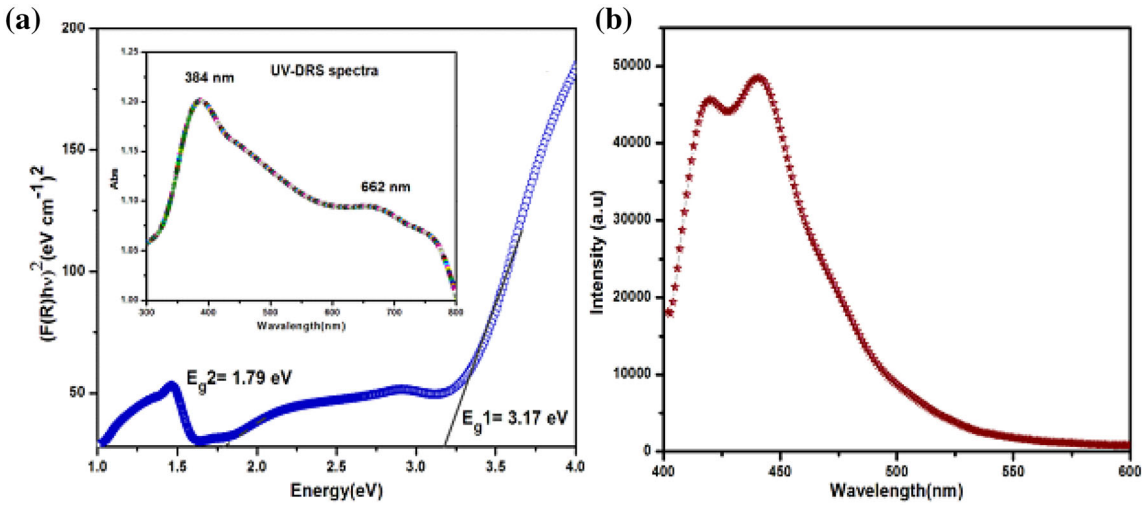

Figure 12. (**a**) KM plot, UV–DRS spectrum (inset) and (**b**) PL spectrum of nano $ZnCo_2O_4$.

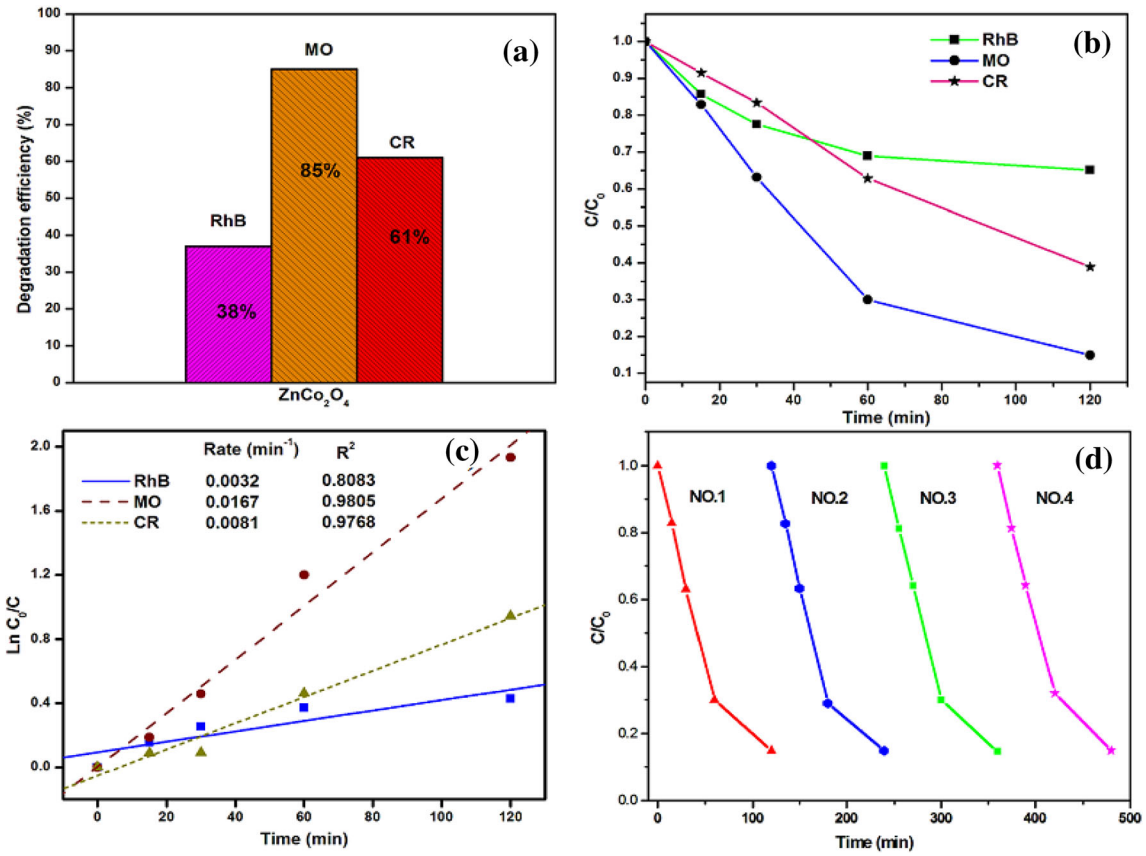

Figure 13. (**a**) Degradation performance of catalyst on RhB, MO and CR dyes, (**b**) change in dye concentration with respect to time, (**c**) kinetic plot for photodegradation and (**d**) recyclability of nano $ZnCo_2O_4$ on degradation of MO dye.

The catalyst shows different efficiencies for different dyes. The results suggest that the nano catalyst shows better catalytic efficiency for azo dyes than RhB dye. The degradation percentage of azo dyes, such as MO (85%) and CR (61%) were higher than RhB (38%) dye (figure 13a). During dye degradation process, azo dyes formed inorganic anion SO_4^{2-} with hydroxyl radical (OH*). An additional fact is that this process takes place faster and increases the rate of cleavage of the chromophore in azo dyes. Compared to RhB, azo dyes experienced higher degradation which

specifies the absence of anchoring group SO_4^{2-} in rhodamine B-based dyes to enhance the photocatalytic degradation [47–50]. In the case of azo dyes, MO (mono azo) encountered faster degradation than CR (diazo) dye. Degradation of these dyes were instigated by the electrophilic cleavage of chromophoric azo (−N=N−) bond in the naphthalene ring. Thus, the dye that contains more azo bonds in its structure, will take a longer time to get degraded [51,52]. These observations validate the proposed direct relationship between degradation efficiency and the number of chromophoric azo bonds (−N=N−) attached.

Figure 13b depicts the C/C_0 relation which describes the catalytic efficiency of the sample, where C_0 is the initial concentration of dye and C is the concentration of a pollutant at time t. The kinetics of photocatalytic reactions can be expressed in terms of the Langmuir–Hinshelwood (L–H) model [53].

$$\ln(C|C_0) = k_{\text{app}}t,$$

where k_{app} is the apparent pseudo-first-order reaction rate constant and t the reaction time. The pseudo-first-order rate constant is derived from the slope of the plot between $\ln(C/C_0)$ and irradiation time is shown in figure 13c. Nano $ZnCo_2O_4$ catalyst degrades azo dyes MO (1.67×10^{-2}) and CR (8.1×10^{-3}) and RhB (3.2×10^{-3}) at different rates. The catalyst has the highest rate constant of 0.0167 min^{-1}, which proves as a model catalyst in this study.

4.3 *Stability and recycle of nano $ZnCo_2O_4$*

To understand the chemical stability of nano $ZnCo_2O_4$, the recycling process of the catalyst for MO dye was carried out by repeating four consecutive experiments for a total duration of 8 h. The magnetization curve exhibits that the nano $ZnCo_2O_4$ is ferromagnetic and it can be recovered by the external magnet (figure 11). After the recovery, the sample was filtered and dried for degradation of MO dye recycling process. Based on the results (figure 13d), the nano $ZnCo_2O_4$ photocatalyst exhibits high chemical stability and recycling ability.

5. Conclusion

In summary, nano $ZnCo_2O_4$ has been synthesized by co-precipitation and followed by thermal decomposition of the precursor at 400°C to explore the structural, textural, optical, magnetic and chemical state properties. XRD pattern of prepared metal oxide was indexed to cubic spinel structure and predominantly oriented in (311) plane with a crystalline size of 17 nm and the findings were further acknowledged by SEM, HRTEM and SAED pattern. Nano $ZnCo_2O_4$ with smaller size and high specific surface area degrades MO, CR and RhB dyes to 85, 61 and 38%, respectively. Based on the findings, it has been concluded that the synthesized catalyst was found to degrade azo dye faster than RhB under similar reaction conditions due to the anchoring sulphonic group on the catalyst surface. Degradation of mono azo dye faster than diazo dye indicates the number of chromophoric azo bonds present in the azo dye which determined the degradation rate.

Acknowledgement

We are thankful to Kongunadu Arts and Science College for providing facilities. We also express our huge gratitude to CIT (Coimbatore), SAIF (Cochin), IIT (Madras), Karunya University (Coimbatore), Amrita Centre for Nanosciences and Molecular Medicine (AIMS, Cochin), CSIR – National Institute for Interdisciplinary Science and Technology (NIIST) Thiruvananthapuram, and BIT University (Bangalore) for providing instrument services.

References

[1] Torretta V, Katsoyiannis I, Collivignarelli M C, Bertanza G and Xanthopoulou M 2020 *MATEC Web Conf.* **305** 00090
[2] Hu X, Lei L, Chen G and Yue P L 2001 *Water Res.* **35** 2078
[3] Li X, Yu J, Li G, Liu H, Wang A, Yang L *et al* 2018 *J. Colloid Interface Sci.* **526** 158
[4] Shehzadi M, Afzal M, Khan M U, Islam E, Mobin A, Anwar S *et al* 2014 *Water Res.* **58** 152
[5] Shahmoradia B, Pordela M A, Pirsaheb M, Malekia A, Kohzadia S, Gongd Y *et al* 2017 *J. Desalin. Water Treat.* **88** 200
[6] Gnanaprakasam A, Sivakumar V and Thirumarimurugan M 2016 *Water Sci. Technol.* **74** 1426
[7] Bhattacharyya K G and Sarma A 2003 *Dyes Pigm.* **57** 211
[8] Asghar A, Raman A A A and Daud W M A W 2015 *J. Clean. Prod.* **87** 826
[9] Mondal S, Purkait M K and De S 2018 *Advances in dye removal technologies*. Springer, Singapore
[10] Chaudhary A, Mohammad A and Mobin S M 2018 *Mater. Sci. Eng.: B* **227** 136
[11] Zhang T, Zhu H and Croue J P 2013 *Environ. Sci. Technol.* **47** 2784
[12] Mendret J, Hatat-Fraile M, Rivallin M and Brosillon S 2013 *J. Sep. Purif. Technol.* **111** 9
[13] Belver C, Bedia J, Gomez-Aviles A, Penas-Garzon M and Rodriguez J J 2019 *Nanoscale Mater. Water Purif.* 581, doi: https://doi.org/10.1016/B978-0-12-813926-4.00028-8
[14] Yang X, Chen W, Huang J, Zhou Y, Zhu Y and Li C 2015 *Sci. Rep.* **5** 10632
[15] Letsholathebe D, Thema F T, Mphale K, Mohamed H E A, Holonga K J, Ketlhwaafetse R *et al* 2020 *Mater. Today: Proc.* **36** 499
[16] Gonçalves P F, Paganini M, Armillotta P, Cerrato E and Calza P 2019 *J. Environ. Chem. Eng.* **7** 103475
[17] Sun Yoo P, Amaranatha Reddy D, Jia Y, Eun Bae S, Huh S and Liu C 2017 *J. Colloid Interface Sci.* **486** 136
[18] Radha B, Rathi R, Lalithambika K C, Thayumanavan A, Ravichandran K and Sriram S 2018 *J. Mater. Sci.: Mater. Electron.* **16** 13474

[19] Mohan R, Krishnamoorthy K and Kim S J 2012 *Solid State Commun.* **152** 375
[20] Raja K, Ramesh P S and Geetha D 2014 *Spectrosc.* **120** 19
[21] Boxi S S and Paria S 2014 *RSC Adv.* **4** 37752
[22] Verenkar V M S, Rane K S and Sawant P Y 1999 *J. Mater. Sci. Mater. Electron.* **10** 133
[23] Rane K S, Verenkar V M S, Pednekar R M and Sawant P Y 1999 *J. Mater. Sci. Mater. Electron.* **10** 121
[24] Porob R A, Khan S Z, Mojumdar S C and Verenkar M S 2006 *J. Therm. Anal. Calorim.* **86** 605
[25] More A and Verenkar V M S 2006 *Inorganic materials: recent advances* (New Delhi: Narosa Publishing House) p 230
[26] Stella C, Soundararajan N and Ramachandran K 2015 *AIP Adv.* **5** 087104
[27] Anandha Babu G, Ravi G and Hayakawa Y 2014 *Appl. Phys. A* **119** 219
[28] Gawas U B, Verenkar V M S and Mojumdar S C 2011 *J. Therm. Anal. Calorim.* **104** 879
[29] Rane K S and Verenkar V M S 2001 *Bull. Mater. Sci.* **24** 39
[30] Borker V, Karmali R and Rane K 2014 *Eur. Chem. Bull.* **3** 520
[31] Vikram L and Sivasankar B N 2007 *Thermochim. Acta* **452** 20
[32] Vogel A I 1989 *A textbook of quantitative chemical analysis*, 5th edn (London: Longman) p 384
[33] Braibanti A, Dallavalle F, Pellinghelli M A and Leporati E 1968 *Inorg. Chem.* **7** 1430
[34] Gonsalves L R, Mojumdar S C and Verenkar V M S 2010 *J. Therm. Anal. Calorim.* **100** 789
[35] Gawas U B and Verenkar V M S 2013 *Thermochim. Acta* **556** 41
[36] Zhu Y, Cao C, Zhang J and Xu X 2015 *J. Mater. Chem.* **A3** 9556
[37] Qiu Y, Yang S, Deng H and Li W 2010 *J. Mater. Chem.* **20** 4439
[38] Wei X, Chen D and Tang W 2007 *Mater. Chem. Phys.* **103** 54
[39] Barakat N A M, Khil M S, Sheikh F A and Kim H Y 2008 *J. Phys. Chem. C* **112** 12225
[40] Matthias T, Katsumi K, Alexander V N, James P O, Francisco R, Jean R *et al* 2015 *Pure Appl. Chem.* **87** 1051
[41] Mariappan C R, Kumar R and Prakash G V 2015 *RSC Adv.* **5** 26843
[42] Pang M J, Jiang S, Long G H, Jia Y, Han W, Wang B B *et al* 2016 *RSC Adv.* **6** 67839
[43] Van H N, Charmaine L and Jae-Jin S 2016 *Mater. Lett.* **170** 105
[44] Varghese B, Hoong T C, Yanwu Z, Reddy M V, Chowdari B V R, Wee A T S *et al* 2007 *Adv. Funct. Mater.* **17** 1932
[45] Malkeshkumar P, Arvind C, Indrajit M, Joondong K and Abhijit R 2016 *Nanoscale* **8** 2293
[46] Pal J and Chauhan P 2010 *Mater. Charact.* **61** 575
[47] Abdullah M A, Muhammed S A A, Tariq A A T and Abdullah D A T 2011 *J. Saudi Chem. Soc.* **15** 121
[48] Sun M, Han X and Chen S 2019 *Mater. Sci. Semicond. Process.* **91** 367
[49] Liu Y, Chen X, Li J and Burda C 2005 *Chemosphere* **61** 11
[50] Hemamalini S and Manimekalai R 2020 *J. Coord. Chem.* **73** 3431
[51] Anku W W, Oppong S O, Shukla S K and Govender P P 2016 *Acta Chim. Slov.* **63** 380
[52] Rauf M A, Meetani M A and Hisaindee S 2011 *Desalination* **276** 13
[53] Galindo C, Jacques P and Kalt A 2001 *Chemosphere* **45** 997